MARS EXPLORATION ROVER PANORAMIC CAMERA MULTIDIMENSIONAL ANALYSES AND SURFACE SPECTRAL VARIABILITY.

F.P. Seelos IV[1], J.M. Soderblom[2], W.H. Farrand[3], J.R. Johnson[4], J.N. Sohl-Dickstein[2], J.F. Bell III[2], S.W. Squyres[2], R.E. Arvidson[1], R.V. Morris[5], H.Y. McSween[6], W.M. Calvin[7], D.L. Blaney[8], and the Athena Science Team.
[1]Washington University, Dept. of Earth and Planetary Sciences, St. Louis MO 63130; seelos@wunder.wustl.edu, [2]Cornell University, Dept. of Astronomy, Ithaca NY 14853, [3]Space Science Institute, Boulder CO 80301, [4]USGS Branch of Astrogeology, Flagstaff AZ 86001, [5]NASA/JSC, Code SR, Huston TX 77058, [6]University of Tennessee, Dept. of Earth and Planetary Sciences, Knoxville, TN 37996. [7]University of Nevada, Dept. of Geological Sciences, Reno NV 89557, [8]NASA/JPL, California Institute of Technology, Pasadena, CA 91109

Introduction: The Mars Exploration Rover (MER) [1] panoramic camera system (Pancam) [2] has provided surface-based multispectral image data with unprecedented spatial and radiometric fidelity. The spectral coverage of the camera system allows for the discrimination of important Fe^{2+} and Fe^{3+} bearing minerals expected to occur on the Martian surface [3,4]. This paper explores the spatially coherent and structurally consistent spectral variability present at both the Spirit [5,6] and Opportunity [7,8] landing sites using multidimensional analysis of representative Pancam multispectral scenes.

Pancam Specifications: Pancam has two eight position filter wheels sampling the 440 nm to 1000 nm wavelength region with one open filter position and two neutral density solar filters. The filter band passes range from 15 nm to 40 nm FWHM and were selected to sufficiently sample the visible ferric absorption edge, the ~650 nm and 860 – 900 nm ferric oxide absorption features and the ~1000 nm ferrous absorption feature [9].

Image Calibration: Pancam data are corrected for bias, dark current, shutter smear, and flat field effects. The images are then scaled using pre-flight radiometry coefficients to units of W/nm/m^2/sr. If contemporaneous images of the calibration target are available, scaling coefficients are fit to the intensity of the three gray target rings relative to their pre-flight reflectance values. These coefficients are then applied to all relevant image bands resulting in units of R* [9] or I/F after a correction for the solar incidence angle is applied [10].

Methodology: Reflectance spectra acquired from geologic materials tend to have strong band-to-band correlations. For imaging spectrometer data this is manifest as a near unity correlation coefficient in the statistical comparison of image bands for adjacent wavelengths. The primary objective of multidimensional image analysis is to overcome this strong spectral correlation in order to identify the materials that drive the spectral variability in the scene and to map the distribution and relative abundance of these scene endmembers. Multidimensional analysis procedures have at their foundation the treatment of each pixel in an image cube as a vector in an orthogonal vector space. This allows for linear algebra based interrogation of the complete data space.

Gusev Crater: Sol 14 Spirit Pancam imaging sequence p2542 provides a multispectral view of the IDD rock target Adirondack and the surrounding materials (Figure 1). This scene was imaged with five of the six left eye visible and near-infrared filters at a consistent pointing geometry. The resulting {1024, 1024, 5} {sample, line, band} image cube allowed for the implementation of a formal dimension reduction and endmember identification procedure [11,12]. Following the application of a Minimum Noise Fraction [13] transform and Pixel Purity Index [11] ranking procedure, the MNF pixels that lie on the multidimensional mixing hull were plotted in R^3 (Figure 2). Through an iterative selection process the clusters of MNF pixels deemed to be either part of a dominant data mode or at an extrema of the mixing space were tagged as a spectral class. A perspective view of the R^3 data cloud with color-coded classes is shown in Figure 2, and the mean reflectance spectrum for each class is shown in Figure 3. The type localities for each class are indicated by color overlays in Figure 1.

Meridiani Planum: For some multispectral scenes advanced mathematical manipulation of the data is not required to bring the spectral variability to light. Sol 4 Opportunity Pancam sequence p2353 shows a segment of the Opportunity outcrop along with associated surface materials. An enhanced false color composite (L357) (Figure 4) readily displays the spectral diversity in a structurally consistent context. Manually selected spectral classes (Figure 5) show significant variability and provide leverage toward constraining the mineralogy of the geologic materials at hand.

Conclusions: Geologic surface processes at the Gusev landing site have acted to mitigate spectral diversity. In the scene presented, ninety-four percent of the spectral variance is carried in the first 3 MNF bands and only two spectral scene endmembers (excepting shade) were identified: rock and induated soils. The rock endmember type localities include the cleanest portion of Adirondack, a rock shown by Moess-

bauer, APXS and Mini-TES to be of mafic composition. The vast majority of the spectra in the scene lie along inter-endmember mixing trends. The spectral evidence for one dominant rock endmember is being used to help delineate the need for a long distance traverse through the ejecta of Bonneville crater with the hope of identifying additional rock types excavated by the impact.

Although Opportunity has only been in operation for 14 sols, the spectral diversity at the Meridiani Planum landing site is readily apparent and the scene endmembers are easily identified. At this time systematic data sets are still being acquired and additional spectral variability analyses will be presented at the conference.

Acknowledgements: We would like to thank the JPL MER engineering team, everyone who participated in the preflight camera calibration effort, and the Cornell calibration crew.

References: [1] Squyres S.W. (2004) LPSC. [2] Bell J.F. III (2004) LPSC. [3] Bell J.F. III (1996) Mineral Spectroscopy, A Tribute to Robert G. Burns, Spec. Pulb. Gochem. Soc., 5. [4] Soderblom L.A. (1992) Mars, [5] McSween H.Y. (2004) LPSC. [6] Malin M.C. (2004) LPSC. [7] Morris R.V. (2004) LPSC. [8] Arvidson R.E. (2004) LPSC. [9] Reid R.J. (1999) JGR, 104, E4, p. 8907-8925. [10] Bell J.F. III (2003) JGR, 108, E12, 8063-8093. [11] Boardman J.W. (1995) Fifth JPL Airborne Earth Science Workshop, JPL publication 95-1, v. 1, p. 23-26. [12] Krause F.A. (1995) Proceedings of the 2nd International Airborne Remote Sensing Conference and Exhibition, v. I, p. I-211 – I-246. [13] Green A.A. (1988) IEE Transactions on Geoscience and Remote Sensing, v. 26, No. 1, p. 65-74

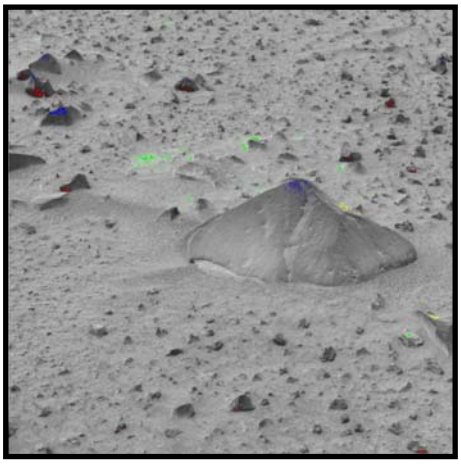

Figure 1. Single band image (L2 = 753 nm) from Sol 14 spirit sequence p2542. Localities of spectral endmember classes are indicated by color overlays.

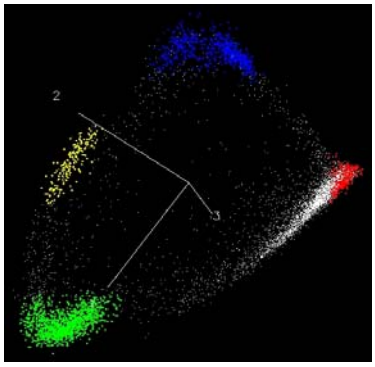

Figure 2. Multidimensional MNF mixing space for the multispectral scene shown in Figure 1. The scene spectral classes appear as pixel clusters in this projection of left-eye data.

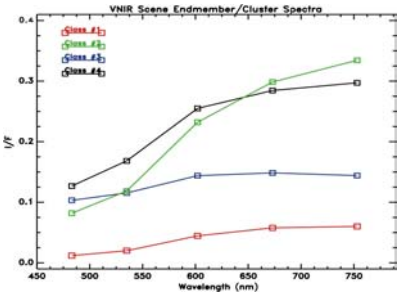

Figure 3. Mean spectra for the classes shown in Figure 1 and Figure 2. The spectral classes for this scene map spatially to #1. shade, #2. indurated soils, #3. rock, and #4. dusty or coated rock. Class #4 is shown as yellow in Figure 1 and Figure 2.

Figure 4. False color composite (L357) (L3 = 673 nm; L5 = 535 nm; L7 = 432 nm) of Sol 4 Opportunity sequence p2353. The type localities of the spectra shown in Figure 5 are indicated by the associated plot symbol.

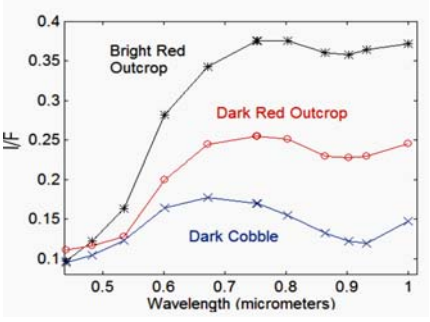

Figure 5. Spectra representative of the diversity shown in Figure 4. These 11-point spectra were compiled by selectively combining the left and right eye image cubes.